Eng. Sci., 2021, **14**, 39–45

Engineered Science

DOI: https://dx.doi.org/10.30919/es8d1169

Broadband and High-efficiency Linear Polarization Converter Based on Reflective Metasurface

Yaxian Guo,[1] Jianchun Xu,[1, 2,*] Chuwen Lan[1, 2] and Ke Bi[1]

Abstract

A linear polarization converter based on metasurface operating in reflection mode was demonstrated. Simulated results indicate that the polarization conversion ratio (PCR) of the polarization converter is more than 90% in the range of 4.73-10.93 GHz. The experiment results are well consistent with the simulated results. Moreover, the bandwidth of linear polarization converter can be tuned by metal patch length and T-shaped slot width. The converter has angular stability below 36° and polarization insensitivity under the *x*- and *y*-polarized incidence waves, which makes it promising for applications in orbital angular momentum beam generators and beam steering systems.

Keywords: Polarization conversion; Broadband; Metasurface.
Received: 10 December 2020; Accepted: 11 January 2021.
Article type: Research article.

1. Introduction

Metasurfaces, as two-dimensional counterparts of metamaterials, have achieved many exotic properties and have been employed in many different applications, such as absorbers, filters, phase shifters, temperature sensors, superlens, and polarization converters from microwave band to optical fields.[1-10] Among these applications, metasurface polarization converters (MPCs) in controlling the polarization states of electromagnetic (EM) waves have attracted extensive attention.[11,12] In contrast to traditional devices, including optical active crystals and liquid crystals,[13-15] MPCs are thin in volume and easy to fabricate.

MPCs tailor phase delays along two orthogonal axes to manipulate the polarization of incident EM waves.[16,17] High polarization conversion ratio (PCR) and wide bandwidth are important for the practical applications of MPCs. In order to obtain wideband characteristics, research efforts have been made to design and optimize MPCs.[18-22] The commonly used technique is by placing one or more resonators to excite multiple resonance modes in the horizontal direction. By using the superposition of multiple metal-dielectric structures in the vertical direction is another main method to enhance the bandwidth of the MPCs. In contrast, the first method has crucial merits of thinner thickness. For instance, Song *et al.* presented a wideband and wide-angle polarization converter based on metallic-dielectric grating structure.[23] Zhou *et al.* proposed a wideband polarization converter with metal gratings embedded in the dielectric layer to obtain optical feedback effect for broadband enhancement.[24] However, the PCR is not high at some frequency ranges, or processing is complex.

In this work, we proposed a linear polarization converter based on reflective metasurface at microwave frequencies. The unit cell of the proposed metasurface consists of a rectangular patch with two T-shaped slots. This structure can simultaneously generate three resonance modes, and the EM coupling between them results in wide bandwidth of the converter. Both the simulations and experiments demonstrated that the converter can effectively convert the linearly polarized incident waves into orthogonal ones.

2. Structure design and principle

Fig. 1(a) depicts the schematic diagram of MPC formed by the periodic arrangement of the unit cell in the *xoy* plane. The MPC is illuminated by *y*-polarized incident EM waves. As shown in Fig. 1(b), the metasurface unit cell is comprised of a copper ground plate, an F4B substrate, and a rectangular metallic structure with two identical T-shaped slots which can

[1] *State Key Laboratory of Information Photonics and Optical Communications, School of Science, Beijing University of Posts and Telecommunications, Beijing 100876, China.*

[2] *Beijing University of Posts and Telecommunications Research Institute, Shenzhen 518057, China.*

* *Email:* Jianchun_xu@bupt.edu.cn (J. Xu)

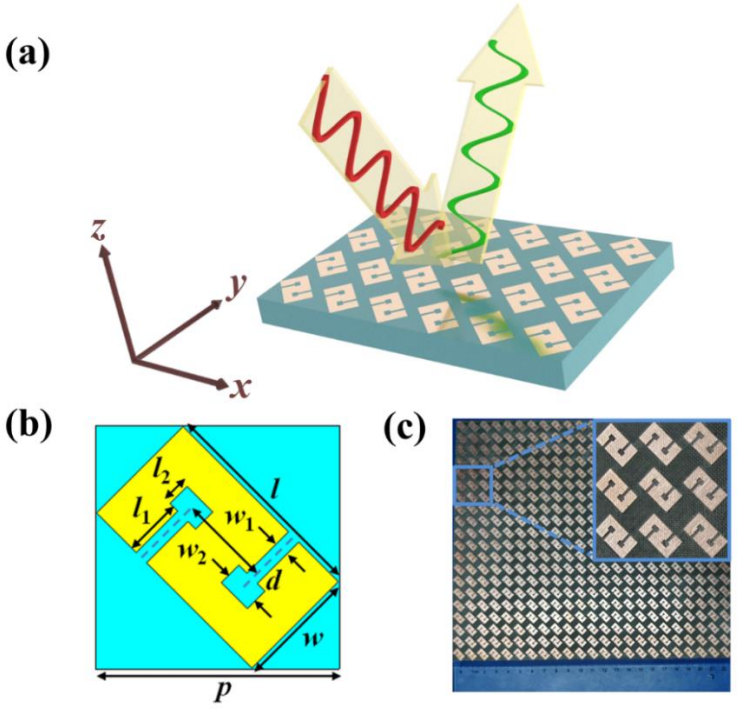

Fig. 1 Schematic diagram of (a) the reflective metasurface-based linear polarization converter and (b) unit cell of the metasurface. (c) Photograph of the fabricated reflective metasurface-based linear polarization converter.

be considered as the overlap of two split-ring resonator analogues. The split-ring resonator is used to generate a certain phase accumulation to realize polarization conversion.[25] The two split-ring resonator analogues are equivalent to the introduction of multiple capacitances and inductances in the structure, and the desired frequencies are obtained by selecting appropriate parameter values. The period of the metasurface structure is p = 10 mm. The metasurface is manufactured on the dielectric substrate with a permittivity of 3.5, a loss tangent tanδ of 0.002, and a thickness of 4.0 mm. The thickness of the metallic pattern and copper ground plane is 0.035 mm. Two T-shaped slots with the same structure parameters are etched on the rectangular patch. In this work, w_1 = 0.6 mm, w_2 = 1.5 mm, l_1 = 2.4 mm, l_2 = 1.0 mm, d = 3.8 mm, width w = 5.0 mm, and length l = 9.0 mm are selected. As shown in Fig. 1(c), a polarization converter sample with a size of 230 mm × 200 mm × 4.0 mm is fabricated.

Commercial time-domain package CST Microwave Studio is used to characterize the reflection spectra of the polarization converter. The boundary conditions are set as periodic along x and y axes, and open along z axis.[26,27] And the proposed MPC is illuminated by a plane wave with the electric field polarized along y axis. In Fig. 2(a), the numerical simulations of the reflection coefficients for co-polarization (r_{yy}) and cross-polarization (r_{xy}) are displayed, where $r_{yy} = |E_{yr}|/|E_{yi}|$ and $r_{xy} = |E_{xr}|/|E_{yi}|$.[28] E_{yi} and E_{yr} denote the electric field of the y-polarized incident and reflected EM waves, respectively. E_{xr} denotes the electric field of x-polarized reflected EM waves. The simulated results show that co-polarized reflection

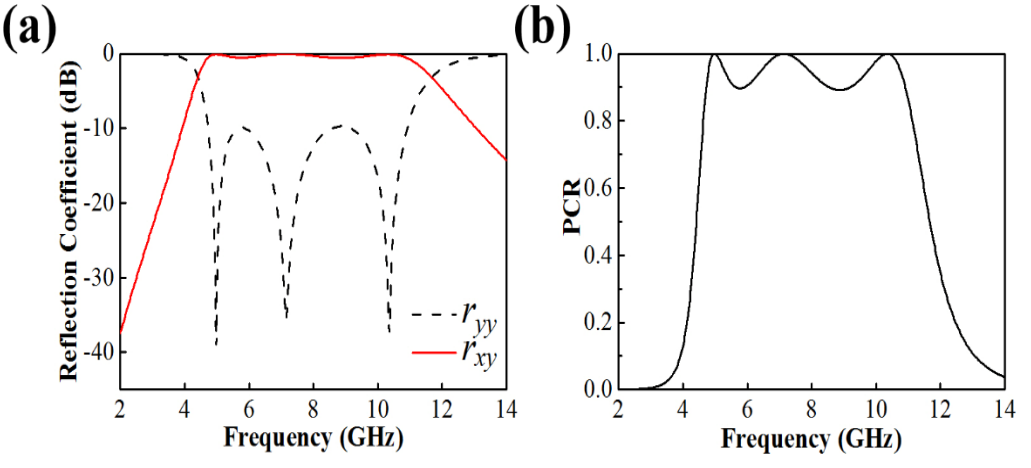

Fig. 2 Simulated (a) reflection coefficients and (b) polarization conversion ratio (PCR) of the reflective metasurface-based linear polarization converter.

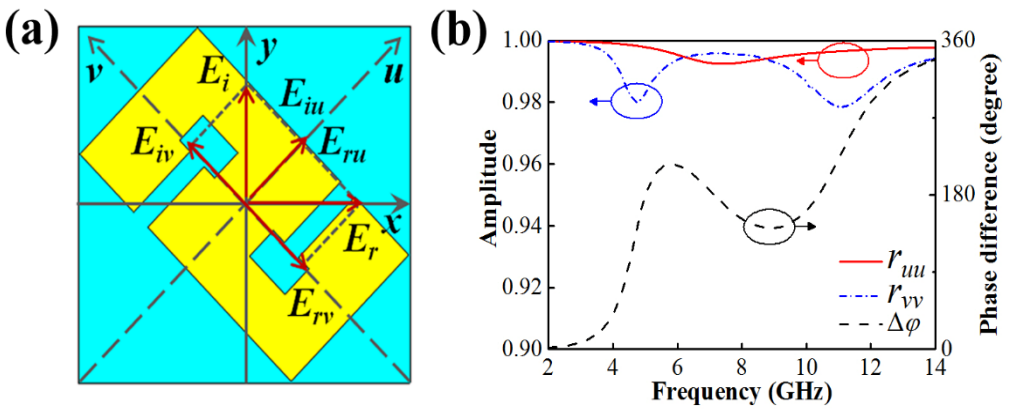

Fig. 3 (a) Schematic diagram of the metasurface unit cell. (b) Reflected amplitudes and phase difference of the metasurface unit cell in the *u*-*v* coordinate system.

coefficient is smaller than -10 dB and cross-polarized reflection coefficient is larger than -1 dB from 4.73 GHz to 10.93 GHz under normal incidence of *y*-polarized waves. The polarization conversion ratio of the proposed structure can be calculated as PCR = $r_{xy}^2/(r_{xy}^2 + r_{yy}^2)$. If r_{yy} is closer to 0 and r_{xy} is closer to 1, the purity of PCR will be larger. Fig. 2(b) shows that the PCR is higher than 90% within the frequency range of 4.73-10.93 GHz. In particular, three polarization conversion peaks respectively appear at 4.98 GHz, 7.15 GHz, and 10.36 GHz, which manifests *y*-polarized waves can be nearly completely converted into *x*-polarized ones at resonance frequencies.

To theoretically analyze the operating principle of the proposed polarization converter, we define a new set of coordinate system, namely the *u*-*v* coordinate system, where *u* and *v* axes are rotated 45° around *y* axis as shown in Fig. 3(a). When EM waves illuminate the planar structure, they are split into two components E_{iu} and E_{iv}. It can be described as following:

$$E_i = \begin{pmatrix} E_{iu} \\ E_{iv} \end{pmatrix} \quad (1)$$

Similarly, the reflected EM waves are depicted as:

$$E_r = \begin{pmatrix} E_{ru} \\ E_{rv} \end{pmatrix} \quad (2)$$

Here, $E_{iu} = |E_{iu}|e^{j\varphi}$, $E_{iv} = |E_{iv}|e^{j\varphi}$. E_{ru} and E_{rv} represent the components of reflected waves along *u* and *v* directions. According to the Jones matrix,[29,30] the relationship between incident waves and reflected waves can be described as:

$$\begin{pmatrix} E_{ru} \\ E_{rv} \end{pmatrix} = \begin{pmatrix} r_{uu} & r_{uv} \\ r_{vu} & r_{vv} \end{pmatrix} \begin{pmatrix} E_{iu} \\ E_{iv} \end{pmatrix} \quad (3)$$

Here, co-polarized reflection coefficients are $r_{uu} = |r_{uu}|e^{j\varphi_{uu}}$, $r_{vv} = |r_{vv}|e^{j\varphi_{vv}}$, cross-polarized reflection coefficients are $r_{uv} = |r_{uv}|e^{j\varphi_{uv}}$, $r_{vu} = |r_{vu}|e^{j\varphi_{vu}}$.

Fig. 3(b) shows that the amplitudes of r_{uu} and r_{vv} are approximately 1. Hence, based on conversion law, we conclude that the values of r_{uv} and r_{vu} are close to 0. In Fig. 3(b), phase difference is expressed as $\Delta\varphi = \varphi_{uu} - \varphi_{vv}$, where $\varphi_{uu} = \arg(r_{uu})$, $\varphi_{vv} = \arg(r_{vv})$ and $\Delta\varphi \in [0, 2\pi]$. It is shown that phase difference is about 180° within 4.73-10.93 GHz. Ultimately, the reflected waves ($E_r = E_{iu}e^{j\varphi_{uu}}\hat{u} - E_{iv}e^{j\varphi_{uu}}\hat{v}$) are perpendicular to incident waves ($E_i = E_{iu}\hat{u} + E_{iv}\hat{v}$) at these frequency ranges, which demonstrates that the metasurface has the capability of polarization conversion over a wide band.

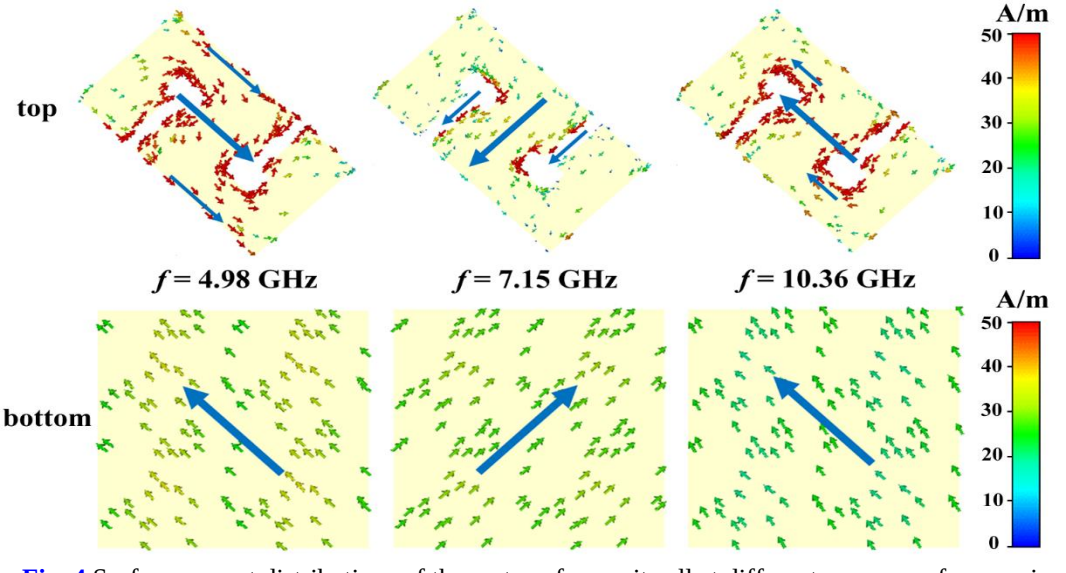

Fig. 4 Surface current distributions of the metasurface unit cell at different resonance frequencies.

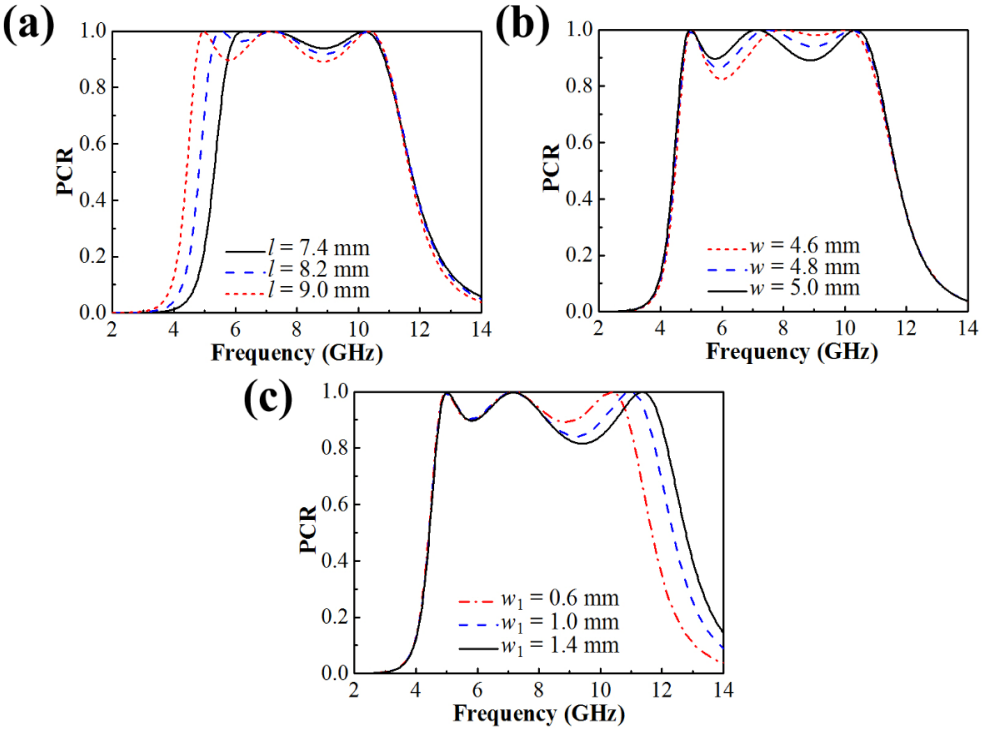

Fig. 5 Simulated polarization conversion ratio of reflective metasurface-based linear polarization converter with a series of (a) *l*, (b) *w*, and (c) w_1.

3. Results and discussion

To further analyze the underlying mechanism of the proposed MPC, the surface current distributions of metasurface unit cell at resonance frequencies of 4.98 GHz, 7.15 GHz, and 10.36 GHz are displayed in Fig. 4. The little blue arrow represents local current and the large blue arrow represents net current, which is the vector sum of the local currents. By identifying net current directions, we find that there are different resonance modes at different resonance frequencies. At 4.98 GHz and 7.15 GHz, the unit cell can be regarded as a magnetic dipole due to the opposite current flow directions on the top and bottom.[31] On the contrary, electric resonance is formed at 10.36 GHz due to the same current flow directions on the top and bottom layers. Therefore, the combination of these magnetic resonances and electric resonance stimulated at different frequencies can result in wide polarization conversion bandwidth.

Furthermore, the dependence of polarization conversion performance on different structure parameters under normal *y*-polarized incidence is investigated. The controlling variable method is adopted during the research process. From Fig. 5(a), when metal patch length *l* increases from 7.4 mm to 9.0 mm, the first resonance frequency redshifts from 6.31 GHz to 4.98 GHz, and the others remain barely changed. The redshift enhances the polarization conversion bandwidth (PCR > 80%), but reduces the conversion efficiency. The simulated PCR curves of the proposed structure with various metal patch width *w* are illustrated in Fig. 5(b). It can be clearly seen that

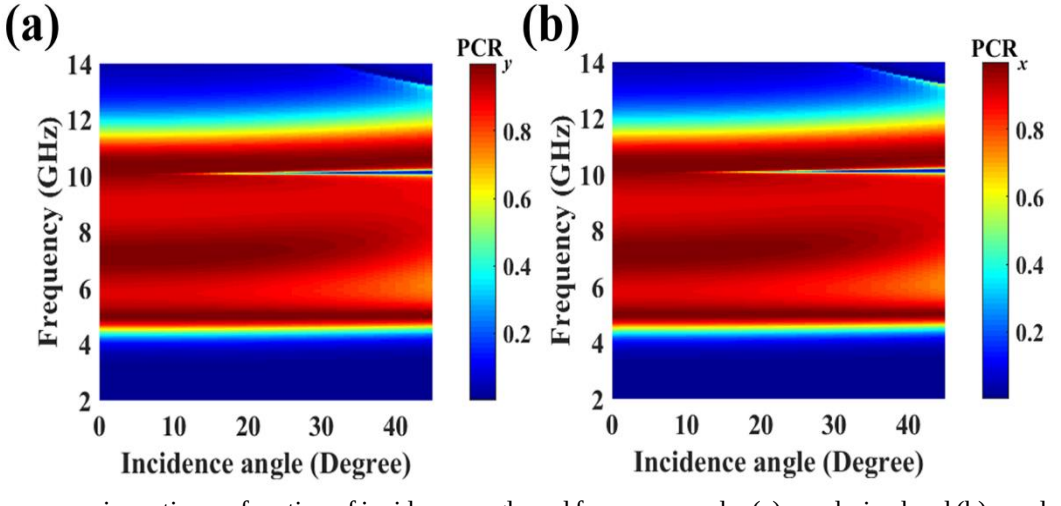

Fig. 6 Polarization conversion ratio as a function of incidence angle and frequency under (a) *y*-polarized and (b) *x*-polarized incidence.

the second resonance frequency is mainly affected by the parameter *w*. As the metal patch width increases, the second frequency moves to the lower frequency. Although the increase in *w* does not affect bandwidth, the PCR between the second resonance frequency and the third one decreases. It is found that as T-shaped slot width w_1 increases, only the third resonance frequency is influenced and shifts to the higher frequency as shown in Fig. 5(c). When w_1 varies from 0.6 mm to 1.4 mm, the corresponding bandwidth changes from 6.4 GHz to 7.4 GHz. However, the conversion efficiency is reduced accordingly. In consequence, the structural parameters can be tuned to obtain appropriate polarization conversion bandwidth and efficiency.

Except for geometrical parameters, external conditions, such as incident EM wave, can also affect the PCR. Therefore, it is necessary to investigate the influence of different polarization states and oblique angles of the incident EM waves on polarization conversion performance, as depicted in Fig. 6. In this figure, PCR_x and PCR_y respectively represent the polarization conversion ratio under the incident waves with *x* polarization and *y* polarization. And their expressions are $PCR_x = r_{yx}^2/(r_{yx}^2 + r_{xx}^2)$, $PCR_y = r_{xy}^2/(r_{xy}^2 + r_{yy}^2)$. According to Figs. 6(a) and 6(b), it is observed that the two polarization conversion spectra are almost identical, which arises from the central symmetry of the structure. When the incidence angle is greater than 15°, PCR_x and PCR_y drop greatly around 10.1 GHz due to the partial absorption.[32,33] This absorption may result from an extra excited resonance between the ground plane and metallic pattern.[34,35] Excluding this frequency point, when the incidence angle is up to 36°, the PCRs are more than 80% in the frequency range (4.7-10.9 GHz). The above results show that the MPC can provide good performance in a wide angle of incidence.

To validate the simulation results, an experimental platform is built, as shown in Fig. 7(a). The measuring equipments including vector network analyzer (VNA) and a pair of 2-18 GHz broadband horn antennas are surrounded by absorbing materials. The metasurface sample is fabricated by using printed circuit board technology and measured by using free-space method.[36-39] Two double ridged horn antennas are used to transmit and receive linearly polarized EM waves respectively. To ensure normal incident plane wave excitation, the two horn antennas have a small angle of about 5° relative to the normal of MPC and satisfy the far field condition. The center of horn antennas is at the same height as the center of the sample. The test system is calibrated by a metal sheet with the same dimension of the sample. When the emitting horn antenna and receiving horn antenna are both horizontally placed, the measured co-polarization reflection result is shown in Fig. 7(b). When the emitting horn antenna is placed horizontally and the receiving horn antenna is vertically placed, the measured cross-polarization result is shown in Fig. 7(c). The placement of two horn antennas is shown in the illustrations. The measured reflection coefficients show that three resonances occur at frequencies of 5.08 GHz, 7.64 GHz, and 10.71 GHz. Based on the measured results, the PCR is

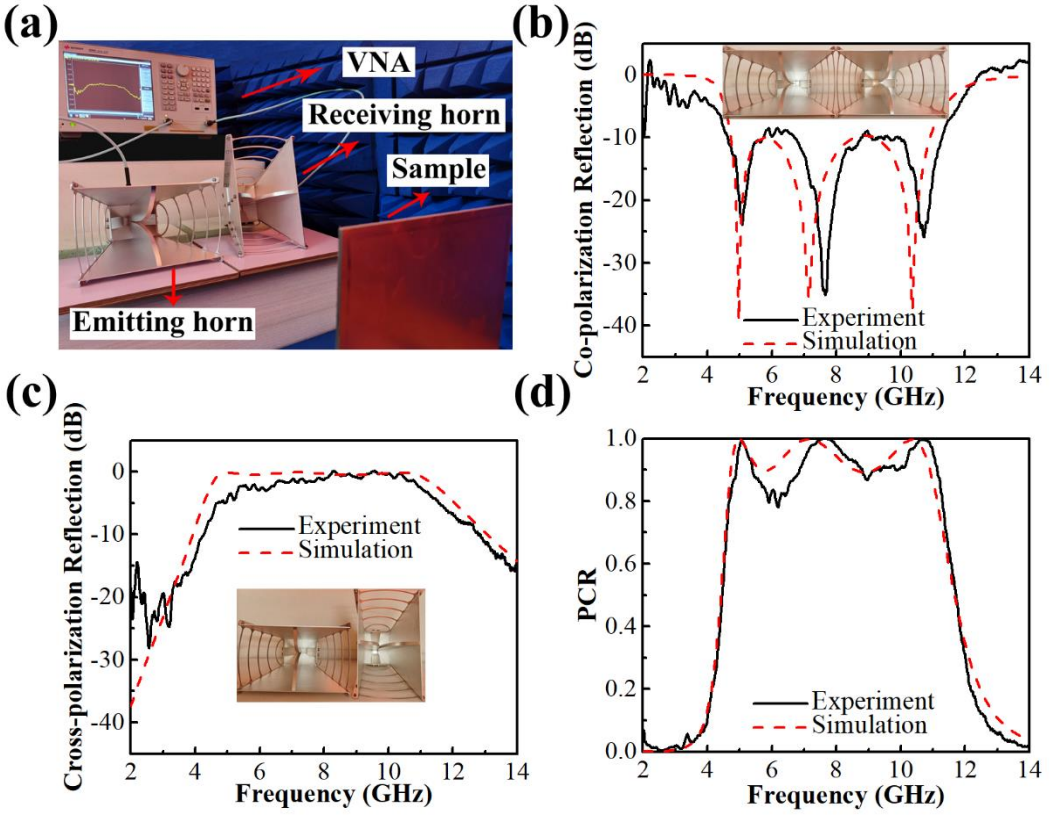

Fig. 7 (a) Measurement setup. Simulated and measured results of (b) co-polarization reflection, (c) cross-polarization reflection and (d) PCR.

computed and shown as the black solid line in Fig. 7(d). It is observed that the PCR is above 0.8 within 4.68-11.29 GHz in measurement and above 0.9 within 4.73-10.93 GHz in simulation. Figs. 7(b)-(d) show that the experimental results are roughly in agreement with the simulated results. There are some discrepancies between the simulated and measured results. For example, these measured resonance frequencies have a little blueshift compared with the simulated results, and the measured value of PCR is lower than 90% at lower frequencies. These are mainly caused by processing errors and size limitation of the sample.[40]

Table. 1 demonstrates the comparison of the proposed MPC with the polarization converters reported in previous literatures. It is obvious that the proposed structure has wideband and high polarization conversion performance.

Table 1 The comparison table of this work with other wideband polarization converters reported in literatures.

Structure	Operating bandwidth (GHz)	Relative bandwidth (%)	PCR
Proposed	4.73-10.93	79.2	>0.9
[23]	4.9-10.4	71.9	>0.71
[31]	5.7-10.3	57.5	>0.9
[41]	8.6-13.9	47.1	>0.9
[42]	9.24-17.64	62.5	>0.9

4. Conclusions

In summary, a broadband linear polarization converter with high polarization conversion efficiency was presented. It is composed of a periodic array of metallic patches with T-shaped slots, a dielectric substrate, and a metal ground plate. Both the simulated and measured results demonstrated that the polarization converter has a wide bandwidth of 4.73-10.93 GHz while maintaining high conversion efficiency. The bandwidth of the metasurface is expanded by the coupling of three resonance frequencies. The center frequency of each resonance peak is mainly affected by metal patch length, metal patch width, and T-shaped slot width, which can be adjusted independently. In addition, the proposed converter keeps high efficiency with a great incidence angle of *x* and *y* polarization waves, which provides a potential way to manipulate the electromagnetic waves' polarization state and obtains wide applications in novel polarization-control devices.

Acknowledgements

We are grateful to the anonymous reviewers for their valuable comments and suggestions. Financial supports from the National Natural Science Foundation of China (Grant Nos. 51972033, 61774020, 61905021, 51802023 and 51802021), Beijing Youth Top-Notch Talent Support Program, Science and Technology Plan of Shenzhen City (Grant No. JCYJ20180306173235924, JCYJ20180305164708625), and Key area research plan of Guangdong (Grant No. 2019B010937001) are also gratefully acknowledged.

Supporting information

Not applicable

Conflict of interest

There are no conflicts to declare.

References

[1] S. G. Carrillo, G. R. Nash, H. Hayat, M. J. Cryan, M. Klemm, H. Bhaskaran, C. D. Wright, *Opt. Express*, 2016, **24**, 13563-13573. doi: 10.1364/OE.24.013563.

[2] J. X. Cai, F. Zhang, M. Zhang, Y. Qu, H. L. Yu, *Sci. Rep.*, 2020, **10**, 14477. doi: 10.1038/s41598-020-71508-7.

[3] Z. L. Han, S. Ohno, Y. Tokizane, K. Nawata, T. Notake, Y. Takida, H. Minamide, *Opt. Express*, 2017, **25**, 31186-31196. doi: 10.1364/OE.25.031186.

[4] J. Z. Han, R. S. Chen, *Opt. Express*, 2020, **28**, 30289-30298. doi: 10.1364/OE.403631.

[5] B. Zhao, J. S. Deng, R. Zhang, L. Y. Liang, B. B. Fan, Z. Y. Bai, G. Shao, C. B. Park, *Eng. Sci.*, 2018, **3**, 5-40. doi: 10.30919/es8d735.

[6] J. C. Xu, Y. N. Hao, K. Bi, R. Zhang, S. G. Huang, J. Zhou, *Eng. Sci.*, 2019, **6**, 30-35. doi: 10.30919/es8d748.

[7] Z. Z. Cheng, Y. Z. Cheng, *Opt. Commun.*, 2019, **435**, 178-182. doi: 10.1016/j.optcom.2018.11.038.

[8] B. Jia, P. Zhu, S. Sun, L. Han, G. Liu, Y. Wang, G.-D. Peng, P. Lu, *IEEE J. Sel. Top. Quant.*, 2019, **26**, 1-6. doi: 10.1109/JSTQE.2019.2939513.

[9] P. F. Lu, *J. Sichuan Norm. Univ.: Nat. Sci.*, 2020, **43**, 1-20. doi: 10.3969/j.issn.1001-8395.2020.01.001.

[10] S. G. Huang, B. L. Guo, Y. N. Liu, *IEEE Commun. Mag.*, 2020, **58**, 13-19. doi: 10.1109/MCOM.001.1900583.

[11] X. Gao, X. Han, W. P. Cao, H. O. Li, H. F. Ma, T. J. Cui, *IEEE T. Antenn. Propag.*, 2015, **63**, 3522-3530. doi: 10.1109/TAP.2015.2434392.

[12] J. C. Zi, Q. Xu, Q. Wang, C. X. Tian, Y. F. Li, X. X. Zhang, J. G. Han, W. L. Zhang, *Appl. Phys. Lett.*, 2018, **113**, 101104. doi: 10.1063/1.5042784.

[13] E. Doumanis, G. Goussetis, R. Dickie, R. Cahill, P. Baine, M. Bain, V. Fusco, J. A. Encinar, G. Toso, *IEEE T. Antenn. Propag.*, 2014, **62**, 2302-2307. doi: 10.1109/TAP.2014.2302844.

[14] C. C. Lin, T. C. Huang, C. C. Chu, V. K. S. Hsiao, *Opt. Mater.*, 2016, **57**, 23-27. doi: 10.1016/j.optmat.2016.04.006.

[15] R. Kowerdziej, J. Wrobel, P. Kula, *Sci. Rep.*, 2019, **9**, 20367. doi: 10.1038/s41598-019-55656-z.

[16] J. Luo, X. Z. Shi, X. Q. Luo, F. R. Hu, G. Y. Li, *Opt. Express*, 2020, **28**, 30861-30870. doi: 10.1364/OE.406006.

[17] X. M. Fu, J. F. Wang, Y. Fan, M. D. Feng, M. B. Yan, Y. F. Li, H. Y. Chen, J. Q. Zhang, S. B. Qu, *Appl. Phys. Lett.*, 2018, **113**, 101901. doi: 10.1063/1.5048247.

[18] M. I. Khan, F. A. Tahir, *J. Appl. Phys.*, 2017, **122**, 053103.

doi: 10.1063/1.4997456.
[19] B. Q. Lin, J. X. Guo, P. Chu, W. J. Huo, Z. Xing, B. G. Huang, L. Wu, *Phys. Rev. Appl.*, 2018, **9**, 024038. doi: 10.1103/PhysRevApplied.9.024038.
[20] F. Long, S. X. Yu, N. Kou, C. Zhang, Z. Ding, Z. P. Zhang, *Microw. Opt. Techn. Let.*, 2020, **62**, 226-232. doi: 10.1002/mop.31991.
[21] S. K. Ghosh, S. Das, S. Bhattacharyya, *Opt. Commun.*, 2021, **480**, 126480. doi: 10.1016/j.optcom.2020.126480.
[22] H. T. Zhang, Y. Z. Cheng, M. L. Huang, *Opto-Electron. Eng.*, 2019, **46**, 180519. doi: 10.12086/oee.2019.180519.
[23] Z. Y. Song, Q. Q. Chu, X. P. Shen, Q. H. Liu, *Front. Phys.-Beijing*, 2018, **13**, 137803. doi: 10.1007/s11467-018-0779-x.
[24] G. C. Zhou, B. Zhu, J. M. Zhao, G. H. Zhu, B. B. Jin, Y. J. Feng, L. Kang, W. W. Xu, J. Chen, P. H. Wu, *Sci. Rep.*, 2017, **7**, 9103. doi: 10.1038/s41598-017-09561-y.
[25] J. P. Fan, Y. Z. Cheng, *J. Phys. D Appl. Phys.*, 2020, **53**, 025109. doi: 10.1088/1361-6463/ab4d76.
[26] Y. Z. Cheng, W. Y. Li, X. S. Mao, *Prog. Electromagn. Res.*, 2019, **165**, 35-45. doi: 10.2528/PIER18112603.
[27] Y. Z. Cheng, J. P. Fan, H. Luo, F. Chen, *IEEE Access*, 2020, **8**, 7615-7621. doi: 10.1109/ACCESS.2019.2962299.
[28] Z. L. Mei, X. M. Ma, C. Lu, Y. D. Zhao, *AIP Adv.*, 2017, **7**, 125323. doi: 10.1063/1.5003446.
[29] S. Jiang, C. Chen, H. L. Zhang, W. D. Chen, *Opt. Express*, 2018, **26**, 6466-6477. doi: 10.1364/OE.26.006466.
[30] M. Piccardo, A. Ambrosio, *Appl. Phys. Lett.*, 2020, **117**, 140501. doi: 10.1063/5.0023338.
[31] J. C. Zhao, Y. Z. Cheng, *Appl. Phys. B*, 2016, **122**, 255. doi: 10.1007/s00340-016-6533-6.
[32] J. Xu, R. Q. Li, J. Qin, S. Y. Wang, T. C. Han, *Opt. Express*, 2018, **26**, 20913-20919. doi: 10.1364/OE.26.020913.
[33] L. B. Zhang, P. H. Zhou, H. P. Lu, L. Zhang, J. L. Xie, L. J. Deng, *Opt. Mater. Express*, 2016, **6**, 1393-1404. doi: 10.1364/OME.6.001393.
[34] X. F. Jing, X. C. Gui, P. W. Zhou, Z. Hong, *J. Lightwave Technol.*, 2018, **36**, 2322-2327. doi: 10.1109/JLT.2018.2808339.
[35] M. Diem, T. Koschny, C. M. Soukoulis, *Phys. Rev. B*, 2009, **79**, 033101. doi: 10.1103/PhysRevB.79.033101.
[36] L. Raimondo, F. De Paulis, A. Orlandi, *IEEE T. Electromang. C*, 2011, **53**, 482-490. doi: 10.1109/TEMC.2010.2051549.
[37] M. Z. Song, P. Smirnov, E. Puhtina, E. Zanganeh, S. Glybovski, P. Belov, P. Kapitanova, *Appl. Phys. Lett.*, 2020, **117**, 083501. doi: 10.1063/5.0012006.
[38] C. C. Lee, D. H. Chen, *Appl. Phys. Lett.*,2007, **90**, 193102. doi: 10.1063/1.2731706.
[39] H. J. Kang, Q. Shao, X. K. Guo, A. Galaska, Y. Y. Liu, Z. H. Guo, *Eng. Sci.*, 2018, **1**, 78-85. doi: 10.30919/espub.es.180312.
[40] J. Xu, R. Q. Li, S. Y. Wang, T. C. Han, *Opt. Express*, 2018, **26**, 26235-26241. doi: 10.1364/OE.26.026235.
[41] H. Y. Chen, J. F. Wang, H. Ma, S. B. Qu, J. Q. Zhang, Z. Xu, A. X. Zhang, *Chinese Phys. B*, 2015, **24**, 014201. doi: 10.1088/1674-1056/24/1/014201.
[42] Q. Zheng, C. J. Guo, H. X. Li, J. Ding, *J. Electromagnet. Wave*, 2018, **32**, 265-273. doi: 0.1080/09205071.2017.1377640.

Author information

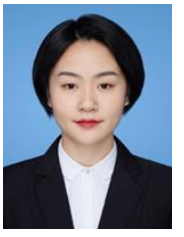

Yaxian Guo *received the B.Sc. degree in physics from Central China Normal University, Wuhan, China, in 2018. She is now pursuing her M.Sc. degree at the Beijing University of Posts and Telecommunications in Beijing, China. Her research interests include polarization control and metasurface.*

Jianchun Xu *received his Ph.D. degree in Electronic Science and Technology from Beijing University of Posts and Telecommunications in 2020. He is now a postdoctor in Beijing University of Posts and Telecommunications. His research interests include metamaterials, orbital angular momentum antenna, and broadband antenna.*

Chuwen Lan *received his Ph.D. degree from the Tsinghua University in 2017. From 2017 to 2019, he was a Postdoctoral Fellow with Beijing University of Posts and Telecommunications. He is currently a lecturer with Beijing University of Posts and Telecommunications. His research interests include metamaterials, THz technology, and optical communications.*

Ke Bi *received his Ph.D. from Nanjing University of Aeronautics and Astronautics in 2012. From 2012 to 2014, he worked as an assistant researcher in Tsinghua University. He is now a professor in Beijing University of Posts and Telecommunications. His research group focuses on information functional materials and devices, electromagnetic metamaterials, and devices.*